Journal of Power Sources 503 (2021) 230030

Contents lists available at ScienceDirect

Journal of Power Sources

journal homepage: www.elsevier.com/locate/jpowsour

A novel measurement technique for parallel-connected lithium-ion cells with controllable interconnection resistance

P. Jocher [a,*], M. Steinhardt [a], S. Ludwig [a], M. Schindler [a], J. Martin [b], A. Jossen [a]

[a] Technical University of Munich (TUM), Institute for Electrical Energy Storage Technology (EES), Arcisstr. 21, 80333 Munich, Germany
[b] BaSyTec GmbH, Öllinger Weg 17, 89176 Asselfingen, Germany

ARTICLE INFO

Keywords:
Current distribution
Virtual parallel connection
Resistance variation
Lithium-ion battery cell
Battery system

ABSTRACT

Due to the broad use of parallel-connected cells across multiple applications, it is essential to understand the current distribution between them. Variations in resistance, temperature and capacity can lead to an inhomogeneous current distribution and have a deleterious influence on ageing and safety. It is therefore crucial to investigate the current distribution within such systems. However, the task of designing a low-complexity test apparatus, that does not itself affect the current measurement, remains incomplete.

This work investigates a novel measurement method to connect cells in parallel with controllable interconnection resistances. Instead of a physical connection, the presented method couples the cell using Kirchhoff's laws via a commercial battery cycler. This connection allows investigation of parallel-connected cells, without influencing factors such as contact resistances or an additional measurement environment.

Further, two studies demonstrate the influence of the additional interconnection resistance caused by the parallel connection of two cells. The results of measurements including a differential voltage analysis show, that the cell current divides according the ratio of the combined cell and interconnection resistance, whilst the open-circuit-voltage influences the shape of the current distribution.

1. Introduction

Lithium-Ion Batteries (LIBs) are used in many different applications and have to fulfil varying power and energy requirements [1]; from consumer electronics, with low energy and power requirements, up to automotive applications, e.g. Audi e-tron, Nissan Leaf, Renault ZOE and Tesla Model 3, to stationary operations where high power and energy are required, series and parallel connections can be used to achieve the desired characteristics [2]. Coupling cells in series raises the voltage of the battery module, although maximum voltage of the battery module is limited by the need for electrical isolation and the cost of semiconductors [3]. Connecting cells in parallel is used to achieve a desired energy. The load of each parallel path is defined by the resistance of the electrical wiring and junction to the cell, the open-circuit-voltage (OCV), the capacity and the internal resistance of the cell.

As such, variations during production, ageing and temperature differences and their effects on the OCV, capacity and the internal resistance can induce inhomogeneous current distribution [4–7]. It is therefore crucial to understand the drivers of the current distribution. With help of test-benches, the measurement of the current through each path in parallel-connected cells, helps to determine the driving forces for convergence and divergence of the current distribution. The typical test-bench challenge is to define and minimise the influencing factors caused by the current measurement. The aim is an accurate and reproducible measurement of the individual cell current. Although we are aware that in commercial settings it can be rather difficult to test, verify, and ensure uniform current distribution in individual paths to another, the researcher goal is understanding the current distribution of parallel connected cells and the development of improved guidelines for commercial applications. Alternative approaches to the problem of battery diagnostics can be found in the work of Wei et al. [8] which discussed a variety of smart battery sensors, containing also innovative current sensors.

To understand the behaviour of parallel-connected cells, many researchers [4–7,9–26] have designed distinct test-benches to measure the current distribution. In any test-bench defined and undefined resistances caused by wiring, interconnections and measurement equipment can adversely effect the current distribution.

A summary of the publications regarding the measurement of the current distribution is presented in Table 1. All test-benches were designed such that measurement equipment and contact areas would

* Corresponding author.
E-mail address: philipp.jocher@tum.de (P. Jocher).

https://doi.org/10.1016/j.jpowsour.2021.230030
Received 10 February 2021; Received in revised form 15 April 2021; Accepted 9 May 2021
Available online 24 May 2021

minimally influence the measured current. For the conventional measurement of the current on each parallel path, contactless, e.g. hall- and fluxgate sensors, as well as contacting sensors, e.g. shunt resistance, were used. Increasing the resistance in parallel paths leads to a more homogeneous current distribution [4,5,12], but the efficiency decreases due to increased ohmic losses. On the other hand, an inhomogeneous resistance ratio between parallel-connected paths leads to a divergent current distribution between parallel conduction paths [4,5,12].

Some of the authors quantified the influence of their interconnection technique, whereas others did not. To better understand their influence upon measurements, values and standard deviation intervals of the resistance of several interconnection techniques can be found in [27–30].

In the studies focussing on the measurement of the current distribution, the researchers investigated at most two parallel (2p) parallel-connected round cells with Lithium Sulphur (LS) and different LIBs cathode materials such as Lithium Iron Phosphate (LFP), Nickel Manganese Cobalt (NMC), Nickel Cobalt Aluminium (NCA) and Lithium Cobalt Oxide (LCO). Additionally, the resistance of the measurement environment is listed in the table, if it was defined in the work. Otherwise not defined (n.d.) is written. The primary goal was to determine the ageing behaviour of parallel-connected cells. Several measurement studies investigated the influence of parameter variations on the current distribution, using real capacity and ohmic resistance differences between the cells [4,5,10,12]. Additionally, measurements provided in [12] show the influence of cable resistances on current distribution.

Brand et al. [4] attempted to construct a defined measurement set-up with low impedances. For the measurement of the current distribution between 2p-connected battery cells the test-bench consisted of six current sensors. Fluxgate- and hall-transducer were used without increasing resistance in any parallel pathways. All in all, Brand et al. were able to determine an additional ohmic resistance of less than 1.5 mΩ per path. Combining test-bench results and simulations, Brand et al. showed, that at the beginning of a current step, the current distribution is dominated by resistances. In contrast, capacity differences affect the current distribution in the long term. Fill et al. [12] described a measurement set-up with adjustable thermal control of cells connected in parallel with an additional resistance of 0.3 mΩ per path and investigated the impact of the resistances on the current distribution within the whole measurement set-up. In this set-up load cables were used as a shunt resistance. Further, they used the measurement set-up to validate a simulation model showing the effects of module design on temperature gradients. Within a subsequent publication, Fill et al. [5] discussed the influence of current distribution, of cell parameter differences and of dynamic current stresses. Hofmann et al. [6] described a measurement set-up, using a shunt current sensor with a resistance of 1.0 mΩ. The test set-up consisted of a copper clamping construction, where cells are connected in parallel using laser welded hilumin plates. The test-bench was used to validate a simulation model for both, CC and dynamic load profiles.

Even though all of the publications in Table 1 produced useable findings, they have a common shortcoming: their measurement set-up influenced the current distribution. Some of the authors described their attempts, at great effort and cost, to determine and reduce each additional parasitic resistance, whereas others do not consider them. As a faulty contact or an unclean test-bench can unbalance the resistance ratio between parallel pathways, whilst the internal resistance of commercial LIBs is in the range of few mΩ, a clean test-bench is indispensable for high-quality experiments.

This work describes a novel measurement technique to connect cells in parallel, that overcomes the problems of additional and undefined resistances due to measurement equipment and contact resistance. Whereas in conventional test-benches cells are connected physically with junctions, Fig. 1(a), this novel technique takes advantage of Kirchhoff's laws, calculating the resulting voltage or current, and connects cells in parallel using a commercial battery cycler, Fig. 1(b) and (c). Therefore, each cell benefits from the 4-wire measurement of the battery cycler, which generates no additional interconnection resistances. For this reason, only the OCV, the capacity and the resistance of the cell itself, as well as its relationship to other cells can influence the current distribution. Each cell is individually connected to the battery cycler using a 4-wire connection, and each cell voltage can be controlled separately. A current pulse is used to determine the voltage across the reference cell and the control unit imposes the same voltage across each cell. Thus, although individually connected to separate voltage sources, a 'virtual parallel connection' is present.

Connecting cells virtually has many advantages, such as coupling and decoupling without touching the cells, scaling to n-parallel constellations, low assembly effort on the test-bench and defined contact resistances. In addition, different cell formats can be investigated with no additional effort.

In this paper, the novel measurement method will first be validated and discussed for CC-, CV- and rest phases using of a conventional test-bench. Next, two studies will show the effect of additional resistances on the measurement. The first study investigates the influence of an inhomogeneous resistance increase within one leg of the parallel paths. Subsequently, the second study examines a homogeneous impedance increase within both parallel-connected paths. Finally, a DVA is used to discuss the relationship between the current distribution and the OCV.

Table 1
Publications regarding current distribution with details on the measurement equipment, the path resistance and the number and chemistry of cells in parallel.

Ref.	Measurement set-up	Number of cells in parallel	Cell format & chemistry	Additional resistance in mΩ per path
[9]	Hall Effect current sensor, undefined wiring	2	18 650 - nickel-based	n.d.
[31]	n.d.	2	18 650 - NCA	n.d.
[4]	Shunt resistance, Fluxgate and Hall Effect current sensor	2	18 650 - NMC	1.5
[10, 21]	Shunt resistance, undefined wiring	4	18 650 - n.d.	10
[11]	Hall Effect current sensor	2 & 3	18 650 - NMC	n.d.
[5,12]	Load cables were used as a shunt	2	Pouch - LCO	0.3
[13]	Shunt resistance	3	Round - LFP	2.15
[14]	Sensors and wiring undefined	2	Round - LFP	n.d.
[15]	Hall Effect current sensor	2, 3 & 4	Pouch - n.d.	n.d.
[16]	Load cables were used as a shunt	4 & 8	26 650 - LFP & 18 650 - LCO	3
[6]	Shunt resistance	2	18 650 - NMC	1
[17]	Shunt resistance	3	Pouch - LS	20
[18]	Shunt resistance	27	18 650 - NMC	25
[7]	Shunt resistance and wiring undefined	5	18 650 - LFP & NMC	3.4
[19]	Shunt resistance, undefined wiring	2 & 4	18 650 - n.d.	5
[20]	Shunt resistance, undefined wiring	2	Pouch - NMC	5
[22, 25]	Contactless sensor, undefined wiring	8	18 650 - n.d.	n.d.
[32]	n.d.	3	Pouch - NCA/LCO	n.d.
[23]	Shunt resistance	2	n.d. - LFP	0.25
[24]	Shunt resistance	Multi tab	Pouch - LFP	2
[26]	Hall Effect current sensor	5	Pouch - LFP	n.d.

2. Experimental

2.1. Cell characteristics

All measurements are performed in a climate chamber (Espec LU-123) at 25 °C with a commercial high energy 3.35 Ah cell

Table 2
Measured capacity and ohmic resistance of the investigated cells in a climate chamber at 25 °C.

Cell	CCCV capacity in Ah	Ohmic resistance in mΩ at 50 % SoC
cell 1	3.288	29.626
cell 2	3.296	32.536
cell 3	3.315	28.413
cell 4	3.344	28.525

(LG INR18650-MJ1). The electrodes are composed of nickel-rich NMC (811) on the cathode and silicon doped graphite (SiC) on the anode side [33,34]. The measurements in this work, unless not otherwise stated, were carried out by a CTS 32 channel battery cycler from BaSyTec GmbH where every cell is connected individually to a channel. According to the data-sheet of the battery cycler used in this work, the voltage sensor is guaranteed to a precision of 1 mV and a resolution of 0.3 mV and the current sensor to a precision of 1 mA and a resolution of 0.250 mA at the voltage and current ranges, used in this work CC periods. At the lower currents used for the DVA and the resting periods, the current measurement exhibits precision and sensitivity values that are correspondingly smaller.

All cells used within this study were initially characterised to determine their capacities and ohmic resistances. The capacity was measured via a constant current constant voltage (CCCV) charge with a CC rate of 0.2 C and a cut off current of 50 mA at 4.2 V. Ohmic impedance was determined at 50 % State of Charge (SoC) using galvano electrochemical impedance spectroscopy (EIS) with a current amplitude of 140 mA on a VMP3 potentiostat from Biologic Science Instruments SAS and was measured as the real-axis intercept of the Nyquist plot.

The cell type used in this work is known to contain variances in capacity and resistance [35–37]. Therefore, for the validation of the virtual parallel connection two cells with resistance spread of 2.9 mΩ and a capacity difference of 8 mAh, cell 1 and cell 2 from Table 2 were used. According to recently published results by Schindler et al. [37], the difference in resistance appears relatively high, since it corresponds to a difference of almost ten times the standard deviation for cells from the respective production batch. On the other hand, the difference in capacity corresponds to only 0.5 times the standard deviation [37].

For the measurements investigating the behaviour of cells with low initial differences in capacity and internal resistance cell 3 and cell 4 (see Table 2) were chosen.

2.2. Measurement principle

Any n-parallel connection can be typified by a simple ECM. Fig. 1(a) represents a simple ECM of a conventional n-parallel connection using a battery cycler in CC mode with as current source and voltage measurement within a 4-wire connection. Within such an ECM, each conduction path $x \in [1, n]$ consists of a cell x, that represents an individual cell including internal resistance and OCV, and a contact resistance, $R_{c,x}$, that stands for any additional resistance caused by contacting, wiring and measurement equipment. Using Kirchhoff's voltage and current laws, the following equations can be defined:

The current, I_x, of path x can be determined by the difference between the total current of the system, I_{tot}, and the sum of the current through all other n parallel paths, according to the Kirchhoff node law, Eq. (1).

$$I_x = I_{tot} - \sum_{y \in [1,n], y \neq x}^{n} I_y \tag{1}$$

Analogously, the voltage across the parallel connection, U_p, can be determined by employing the Kirchhoff loop law, represented by m_1 on Fig. 1(a). This generates Eq. (2).

$$U_p = U_{cell\ y} + I_y \cdot R_{c,y} = U_{cell\ x} + I_x \cdot R_{c,x} \tag{2}$$

Based on Eq. (2), the voltage of the cell x in path x, $U_{cell\ x}$, as a function of cell y, can be determined with Eq. (3).

$$U_{cell\ x} = U_{cell\ y} + I_y \cdot R_{c,y} - I_x \cdot R_{c,x} \tag{3}$$

If all cells are operated by independent battery test channels, and assuming that each channel can read the values of voltage and current from others and use this as a control parameter, it is possible to set up the virtual parallel connection. This is achieved by utilising Eqs. (1) and (3). An example of this is provided in Fig. 1(c) where cell 1 is operated by a current source in respect to Eq. (1) – current I_1 is then used as the setpoint and voltage $U_{cell,1}$ is the feedback parameter that is fed to the control unit. All other n-1 cells are operated by a voltage source corresponding to Eq. (3) and as such, voltage $U_{cell,n}$ is the setpoint and current I_n is the feedback parameter. This means that each cell is operated at the same voltage, as though the cells were in parallel. Further, no undefined contact resistances occur due to the 4-wire connection of each channel. If an additional resistance is desired, the virtual parallel connection can increase the interconnection resistance, $R_{c,x}$, by calculating an ohmic loss in respect to Eq. (3).

The resulting closed-loop control system of n-parallel-connected cells is shown in Fig. 1(b). The forward path corresponds to the path through cell 1 with the additional resistance $R_{c,1}$. Further, the feedback path corresponds to the path through cell 2 with the resistance $R_{c,2}$. The setpoint of the forward-path is the current I_1 and the voltage sensor measures the cell response of cell 1. Combining the calculated voltage drop over the resistance $R_{c,1}$ with the calculated current through path 1, the voltage of the virtual parallel connection, U_p, results. The feedback path of cell 2, controlled by voltage $U_{cell,2}$ results in the current I_2. This current I_2 is used to calculate the voltage drop over the resistance $R_{c,2}$. Any additional parallel path of n cells is calculated in the same manner as the feedback path of cell 2.

Consequently, for a 2p connection, the above defined equations were summarised to two equations. The voltage of cell 2 is controlled as in Eq. (3) and the current of cell 1 is controlled as in Eq. (1). According to Brand et al. [4] an asymmetric resistance ratio influences the beginning of a current pulse in the manner of a typical current divider. The current divider for the 2p connection of this work is given by Eq. (4), based on the ECM on Fig. 1(a).

$$i_2/i_{tot} = \frac{R_{cell,1} + R_{c,1}}{R_{cell,1} + R_{c,1} + R_{cell,2} + R_{c,2}} \tag{4}$$

2.3. Validation of the measurement

The virtual parallel connection described above is validated by a conventional 2p test-bench. This test-bench was designed and validated by Hofmann et al. [6,38]. To allow a better understanding of this work, a short summary is given.

The conventional test-bench of Hofmann et al. is shown in Fig. 2. It consists of a shunt current transducer ① with a resistance of 1.0 mΩ and a temperature coefficient of 30 ppm K^{-1}. Each cell ⑧ is mounted with laser-welded hilumin plates ② and fixed into the copper clamps ⑦. Soldered junctions and wiring ③ are used to connect the shunt resistance ① with the copper clamp ⑦ and the main connector ④. A 24-bit analog digital converter (ADC) measurement board ⑪ is used to measure the current. The current is applied to the main connector ④.

A temperature control unit is also integrated into the test-bench but not used and not mounted in this work. Consequently, the cells in this work are connected without cooler ⑩, Peltier element ⑥ and copper shells ⑤.

For the measurement using the virtual parallel connection, the cells are removed from the conventional test-bench and connected by the individual cell connector ⑨ to an independent channel of the battery cycler. With the 4-wire measurement at the hiliumin plate, the

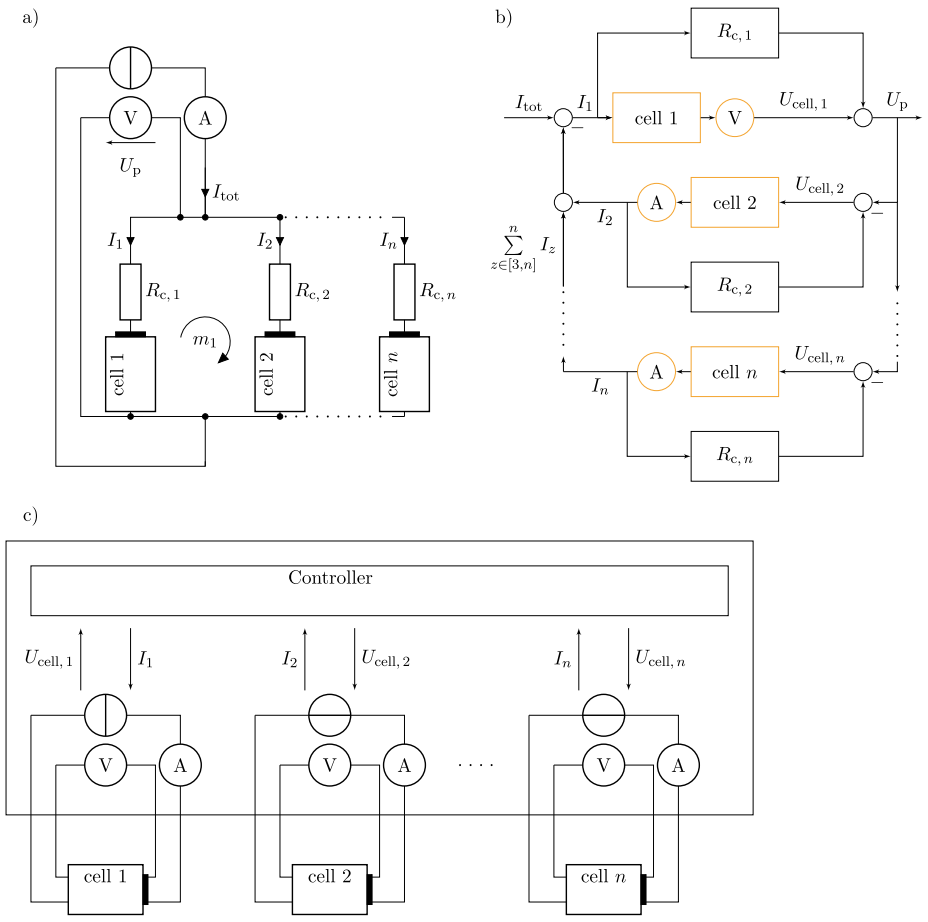

Fig. 1. (a) Simple ECM of a conventional n-parallel connection using a battery cycler in CC mode – current source and voltage measurement – in which each cell represents both the cell and its internal resistance, and a contact resistance, R_c that stands for any additional potential drop due to contacting, wiring and measurement equipment. (b) Closed-loop control system of a virtual n-parallel connection. The forward-path corresponds to the cell 1 with the additional resistance $R_{c,1}$ and the feedback-path is equivalent to the cell 2 (cell n) with the additional resistance $R_{c,2}$ ($R_{c,n}$). All symbols with an orange border refer to physical components. (c) Schematic of the virtual parallel connection within a n-channel battery cycler and physical cells connected to individuals channels via 4-wire technique. The controller calculates the setpoint of any channel with regard to Eqs. (1) and (3). Cell 1 is fed by a current source, see Eq. (1); current I_1 is the setpoint and voltage $U_{cell,1}$ is the feedback parameter. All other n-1 cells are operated with a voltage source, see Eq. (3). Voltage $U_{cell,n}$ is the setpoint and current I_n is the feedback parameter. (For interpretation of the references to colour in this figure legend, the reader is referred to the web version of this article.)

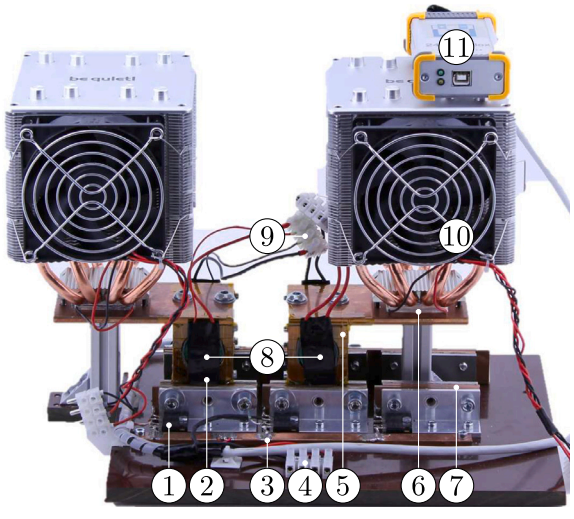

Fig. 2. Conventional test-bench used for the validation of the virtual measurement method; picture taken from [38]. Shunt ①, hilumin plate ②, soldered connection and wiring ③, main 2p connector ④, copper shells - not used in this work ⑤, peltier element - not used in this work ⑥, copper clamp ⑦, cells ⑧, individual cell connector ⑨, cooler - not used in this work ⑩, measurement board ⑪.

resistance of the laser-welded spots from the cell pole to the hilumin plate can be neglected. The measured capacity and ohmic resistance of these cells, as described in Table 2, had been established using this connection.

To ensure that both measurement methods incorporate the same additional resistance of the test-bench, $R_{c,x}$ has to be included in the virtual parallel connection. To define the resistance influence of the conventional test-bench, a hilumin strip was clamped between the two copper clamps, ⑦ on Fig. 2, instead of a physical cell.

Using this measurement set-up, an additional resistance of 2.2 mΩ for each path was determined using a high precision resistance measurement unit from Li.plus GmbH. The additional resistance results from the shunt of 1 mΩ ①, the press contact and the soldered connections as well as the wiring ③ between the main connector ④ and the clamping construction ⑦. Considering the results given in [28], the resistance of a press contact area of 10 mm × 15 mm with brass as the contacting material results in a resistance of about 0.15 mΩ. The remaining resistance of 0.9 mΩ is caused by additional undefined resistances due to soldered connections and wiring. Additional undefined resistances due to the area in the clamp and the welding area may occur.

3. Results and discussion

3.1. Validation of the measurement setup

For the validation of the virtual parallel connection, two test scenarios were chosen. The first test scenario was a CCCV charge and discharge, each at 1 C, and a cut-off current of 100 mA. The second test scenario was a CC charge and discharge at 1 C and a consecutive rest phase of 3600 s after each of the CC phases. The currents are related to the system current, and we would expect that the nominal current per cell should be half of the system current. Both scenarios were repeated over four cycles.

If one aims to compare different measurement methods with each other, it has to be ensured that the current distribution is reproducible and does not change significantly between two consecutive cycles. To calculate the difference between two cycles, x_1 and x_2, the root mean square (RMS) value x_{RMS} can be calculated by Eq. (5) and the maximum difference by Eq. (6). Here, i defines the time-discrete point.

$$x_{\mathrm{RMS}} = \sqrt{\frac{1}{n}\sum_{i=1}^{n}(x_1(i) - x_2(i))^2} \tag{5}$$

$$x_{\mathrm{max}} = \max_{i=1,\dots n} |x_1(i) - x_2(i)| \tag{6}$$

The differences between two consecutive cycles of virtual parallel connection were calculated to be $i_{\mathrm{RMS}} = 0.487\,\mathrm{mA}$ with a maximum value of $i_{\mathrm{max}} = 2.386\,\mathrm{mA}$, whereas the conventional test-bench resulted an $i_{\mathrm{RMS}} = 0.438\,\mathrm{mA}$ and a maximum difference of $i_{\mathrm{max}} = 3.402\,\mathrm{mA}$. Taking the mean current of 1.675 A into account, these differences correspond to maximum deviation of 0.03 % and 0.2 %. For the purposes of comparing the measurement methods, these deviations are deemed to be negligible.

Further, the standard deviation of the sum of both currents over a CC phase is a quality factor of the test-bench and the battery cycler. The noise of the virtual measurement was found to 0.52 mA.

To compare and contrast the two measurement methods, six different phases of a typical LIBs charge–discharge cycle, including CC, CV and resting, were analysed. As described above, an additional resistance of $R_{\mathrm{c},x} = 2.2\,\mathrm{m\Omega}$ was added to each leg of the virtual connection to ensure comparability. Figs. 3 and 4 show the current distribution of both measurement methods over their charge and discharge phases. The orange lines represent the test-bench measurements with a physical interconnection and are labelled with “physical”, whereas the blue lines show the measurements with the virtual parallel connection and are therefore labelled with “virtual”. The solid lines correspond to the current through path 1 and the dashed lines to the current of path 2. The black, dashed line on the subfigure (a) represents the case of a homogeneous current distribution. The C-rate of the y-axis is calculated relative to the nominal capacity of a single cell.

Fig. 3 illustrates the charging behaviour of both methods. The subfigures represent the CC charging phase (a), the CV charging phase (b) and the resting phase (c) for both measurement techniques. For all measurements high qualitative and quantitative compliance is seen. Since both approaches display a high degree of similarity, the virtual rate closely follows the physical test-bench rate.

The lines representing the relative distribution of the charge produced by both methods agree closely. This is shown by the locations of their local minima and maxima and the intersection with the line drawn at 0.5 C. The same cumulative charge per cell is measured by both methods. This result is underlined by an RMS of less than 1.9 mA (0.11 %) for both, CC and CV charging between both measurement methods. Fig. 3(c) illustrates the resting phase after a CC charging.

Fig. 4 shows the discharge behaviour of the two cells connected in parallel. The CC and CV phases are marked with the letters (a) and (b) respectively. As seen in the charging behaviour, the local minima

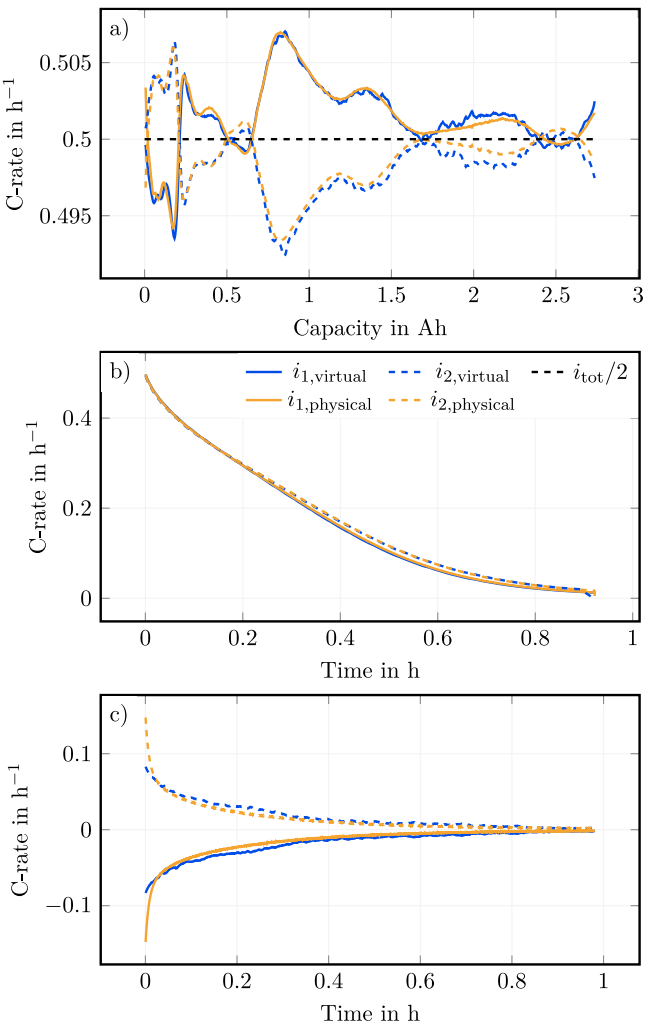

Fig. 3. Validation of the current distribution during charge between the novel measurement method and a conventional test-bench [38]. (a) shows the CC charge with an current of $I_{\mathrm{tot}} = 1\,\mathrm{C}$ and (b) shows the consecutive CV charge to 4.2 V. (c) shows the rest phase after a CC charge. (For interpretation of the references to colour in this figure legend, the reader is referred to the web version of this article.)

and maxima and the intersections of both currents display the same cumulative discharge throughput per path during discharge. Fig. 4(c) represents the rest phase after the CC discharge, where the highest difference occurs during the beginning of the phase. This might be explained as a consequence of the divergent current distribution at the end of the previous phase. Fig. 4(b) and (c) show the greatest differences between both measurement methods with disparities of 138.2 mA for the CV phase and 157.6 mA for the rest phase. Both follow the CC discharge phase, and the highest difference of 72.14 mA occurs during CC discharging at low SoC around 3.2 Ah. It seems that the virtually connected cells are exposed to a slightly higher voltage range, and therefore the current shows higher spreads at the end of the CC discharge phase. Most likely, this is caused by an additional resistance in the virtual test-bench due to an undefined resistance in the clamp contacts of the construction. The influence of such additional resistances is presented later on to underpin the importance of a correctly defined resistance in the measurement set-up. Nevertheless, an RMS of less than 7.5 mA (0.45 %) for both CC and CV discharging can be determined. Table 3 summarises all differences between RMS and maximum current for both test scenarios.

All in all, the comparison of the two measurement methods shows good correspondence between the local minima and maxima of both

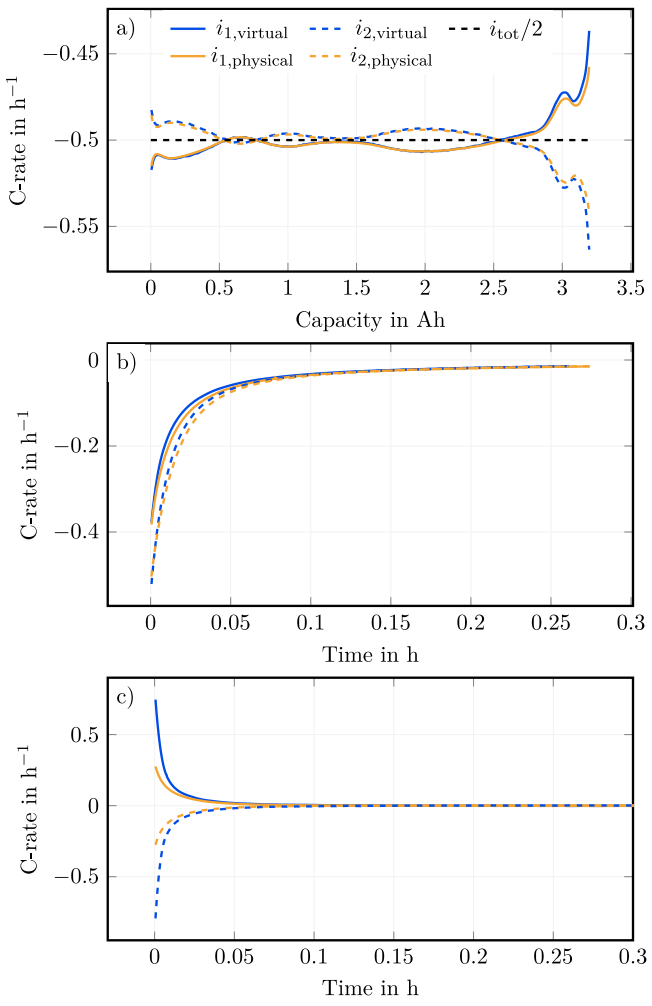

Fig. 4. Validation of the current distribution during discharge between the novel measurement method and a conventional test-bench [38]. (a) shows the CC discharge with an current of $I_{\text{tot}} = 1\,\text{C}$ and (b) shows the consecutive CV discharge to 2.5 V. (c) shows the rest after a CC discharge. (For interpretation of the references to colour in this figure legend, the reader is referred to the web version of this article.)

Table 3
Differences between i_{RMS} and i_{max} in the conventional- and the virtual measurement method in different phases, according to Figs. 3 and 4.

	Fig. 3 - Charge			Fig. 4 - Discharge		
	CC (a)	CV (b)	Rest (c)	CC (a)	CV (b)	Rest (c)
i_{RMS} in mA	1.485	1.838	1.912	7.054	6.444	7.411
i_{max} in mA	14.71	19.76	21.61	72.14	138.2	157.6

measurement methods as well as the intersection points of both currents during CC charging and discharging demonstrating points where the uneven current distribution through the cells was reversed. With these findings, the virtual connection can be used as a measurement method to connect cells in parallel. The presented measurement method should be open to all measurement devices which are capable of dynamic interaction between their channels.

Researchers investigating the ageing of parallel-connected LIBs have reported differing results in regard to the convergence and divergence of the current distribution. Although some discovered convergent current distribution behaviours [10,21], others found the opposite [15,39–42].

Any ageing study of LIBs is complex. Due to the influence of parameter variations, environmental parameters and load profiles on the ageing behaviour [43], a large number of tests are necessary to reach a scientific conclusion [44]. With individual cell connections each cell is connected via the 4-wire technique, therefore no additional resistance occurs and this is increasing the accuracy of the measurement.

Conversely, the interconnection of the cells in a conventional parallel test bench as well as the measurement of the current can introduce additional resistances that can influence the current distribution [12,28,31]. Added to the extra time and effort required to set such test benches up, the virtual parallel measurement represents a quicker and easier method to measure the same quantities. It is also not subject to the distorting effects of the additional resistances. To define possible influences of system parameters two studies are carried out.

3.2. Influence of system parameters

Due to the nature of electrical connection, additional resistances are inevitable in physical applications. In any conventional test-bench, the contact, wiring and measurement resistances increase the influence of the test-bench on the measurement. As described in Section 1, these additional interconnection resistances influence the current distribution and should therefore be minimised. Thus, in the following section, the influence of varying interconnection resistances within the measurement set-up on the current distribution is investigated. The intention is a better understanding of the drivers of inhomogeneous current distribution during measurements with exact additional resistance.

This study addresses the influence of undefined resistances, e.g. due to production variance of the electrical connectors, as well as defined resistances in test-benches, e.g. measurement equipment. The values were chosen with respect to typical additional resistances of conventional test-benches as summarised in Table 1, as well as faulty contact resistances. Hence, the resistance $R_{\text{c},x}$ is set to 0 mΩ, 0.2 mΩ, 0.5 mΩ, 1 mΩ, 2 mΩ and 5 mΩ and measurements were conducted using cell 3 and cell 4, which are described in Table 2. Two 2p studies with additional interconnection resistances are examined by increasing of R_{c}. Study one analyses an increase of $R_{\text{c},2}$, where $R_{\text{c},1}$, is set to 0 mΩ. Study two investigates an increase of the resistance on both paths, such that $R_{\text{c},1} = R_{\text{c},2}$. For both studies the x-axis represents time and not the charge throughput as used in Figs. 3 and 4. This allows a better comparison of the curves due to the inhomogeneous resistance ratio.

Fig. 5 shows CC charging and discharging in the presence of an asymmetric resistance ratio with a homogeneous current through each path of $i_{1/2} = 0.5\,\text{C}$. As expected from Eq. (4), the degree of distribution of the current is determined by the path resistance. This is however not responsible for the alterations in this distribution over time, which remain independent of path resistance. At the marked time intervals, the same maxima and minima are seen for all measurements. A quantitative analysis of the current at different local minima and maxima is illustrated in Fig. 7. The height change in the minima and maxima marked from ① to ⑥ in Fig. 5 corresponds to the ratio of the respective path resistances.

The higher current gap observed for marker ① during discharging can be explained by the SoC dependency of the internal resistance, as noted generally by [45,46] and by Zilberman et al. [47] for this cell type. The resistance is minimal at medium SoC range and increases for both higher and lower SoC. Its maximum values are found at low SoC. This can also be seen in the gradient of marker ① in the current in Fig. 7(a). The higher the internal resistance of both cells, the flatter the resultant gradient, see Eq. (4). Further, the steepness of the OCV influences this phenomenon [6]. Consequently, variations in resistance dominate the current distribution for flatter OCVs, whereas OCV changes become more influential as they become steeper. Therefore it can be stated, that the height of the minima and maxima of the current distribution are mainly dependent on the resistance ratio. In contrast, neither local minima and maxima seen at given cumulative charge throughputs, nor the changes in current distribution between

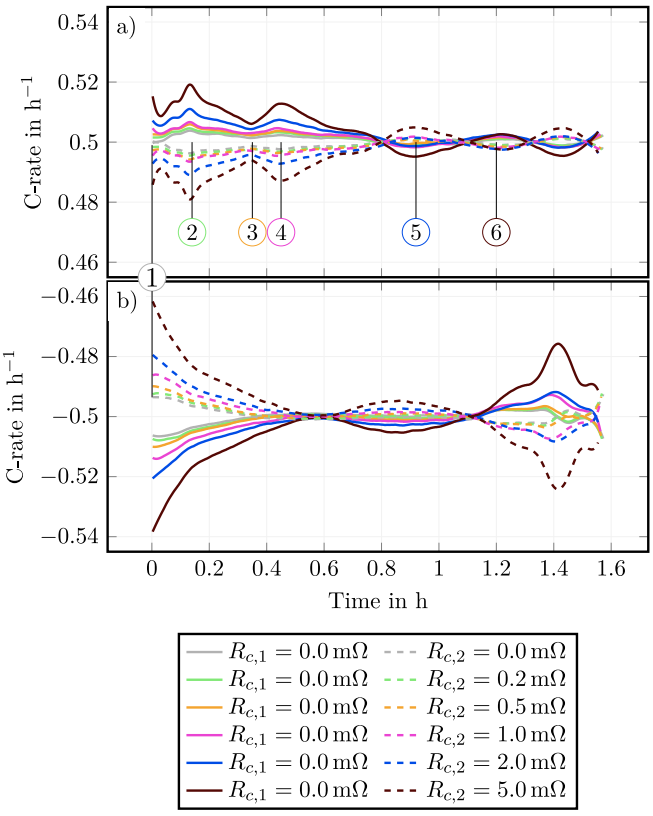

Fig. 5. Current distribution with the virtual parallel connection within inhomogeneous interconnection resistances. The resistance of path 1 was held at 0 mΩ while the interconnection resistance of path 2 was varied from 0 mΩ to 5 mΩ. Measurements were conducted during CC charging in (a) and discharging in (b) with a homogeneous current in each branch of 0.5 C. The marked circles correspond to local minima and maxima and are used in further analyses. (For interpretation of the references to colour in this figure legend, the reader is referred to the web version of this article.)

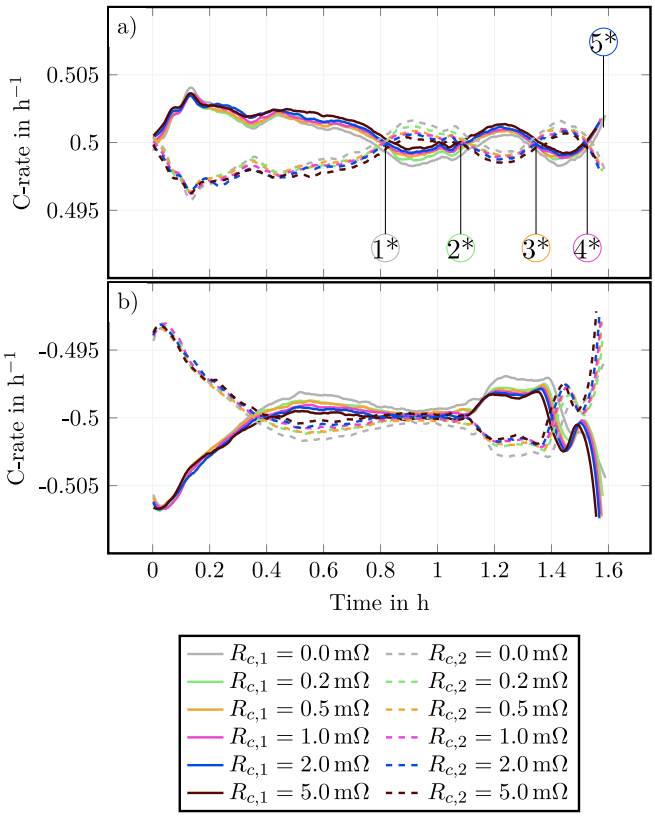

Fig. 6. Current distribution with the virtual measurement method and homogeneous interconnection resistances. The resistance of path 1 and of path 2 was varied from 0 mΩ to 5 mΩ. Measurements were conducted during CC charging in (a) and discharging in (b) with a homogeneous current in each branch of 0.5 C. The marked circles correspond to the intersection points of both currents, which are used in further analyses. (For interpretation of the references to colour in this figure legend, the reader is referred to the web version of this article.)

the cells are affected by the resistance ratios. Instead, the later two factors are dictated by the OCV interaction between the cells.

In a similar manner, the effect of increasing homogeneous path resistance on the current distribution was measured for CC charging and discharging, see Fig. 6. The current distribution with no additional resistance, $R_{c,x} = 0\,\mathrm{m\Omega}$, echos the shape of Fig. 5. As expected, the current is very evenly distributed at the start of the measurement, as Eq. (4) suggests. During charging and discharging, the current distribution depends on the resistance of the paths, while higher additional resistances homogenise the current distribution. Nevertheless, the shape of the current distribution does not change significantly, and the intersection points of both currents only change marginally over the resistance increase.

A closer look at the progress of the intersection points of both currents, marked from ①* to ⑤* on Fig. 6, is given in Fig. 7(b). Here the relative capacity at the intersection points of both currents over all charging cycles with a homogeneous current in each path of $i_{1/2} = 0.5\,\mathrm{C}$ to study the influence of homogeneous resistance based on the first cycle is shown. Measurements were conducted three times at each resistance level. Analysing the behaviour of the intersection points of both currents as the cycles increase, some trends are visible. Intersection points ①* and ③* generally occur at higher capacities as the number of cycles increase, whereas intersection points ②* and ④* generally occur at lower capacities as the number of cycles increase. However ④* correlates with ⑤*, which represents the capacity of the CC fully charged cell. The alteration in the intersections over time may indicate ageing, as reported in [48,49], however this cannot be stated conclusively in this paper.

The same behaviour is also reported by Fill et al. in [12], where the influence of cable resistances was pinpointed within measurements. That paper also showed an independence between the intersection points of the currents and the resistance differences between parallel-connected cells. To analyse this in detail, the current distribution is compared with the DVA in the following paragraphs.

The DVA can be used for chemical investigation [48], as well as to detect degradation mechanisms, where the characteristics of the DVA can be evaluated to determine different ageing contributions as loss of lithium inventory (LLI) and loss of active material (LAM) [50,51]. Hust [18] explained current distribution based on the change of the OCV. With a DVA analysis of 27 parallel-connected cells, regions of an increased importance of the impedances and regions of increased importance of the OCV were noted. According to Hofmann et al. [6] a change in the OCV gradient influences the current distribution by causing an increase or decrease in the OCV differences between the cells. With this in mind, a DVA was carried out in this work during a 2p measurement. As a DVA provides clearer results at lower currents, the system current, i_{tot} was therefore set to 0.1 C [52]. This allowed a deeper analysis of the 2p DVA. The DVA is usually plotted over the capacity or the SoC during a CC charge or discharge. However, because the path current does not remain constant during the 2p measurement, and therefore the DVA of the 2p measurement is plotted over the voltage in this work.

Fig. 8 illustrates the analysis of the current distribution within the DVA. The corresponding DVA is illustrated in Fig. 8(b) and is normalised by the measured capacity, Q_0, as performed by [52]. Additionally, the dashed lines in Fig. 8(b) and (c) were extracted from Sturm

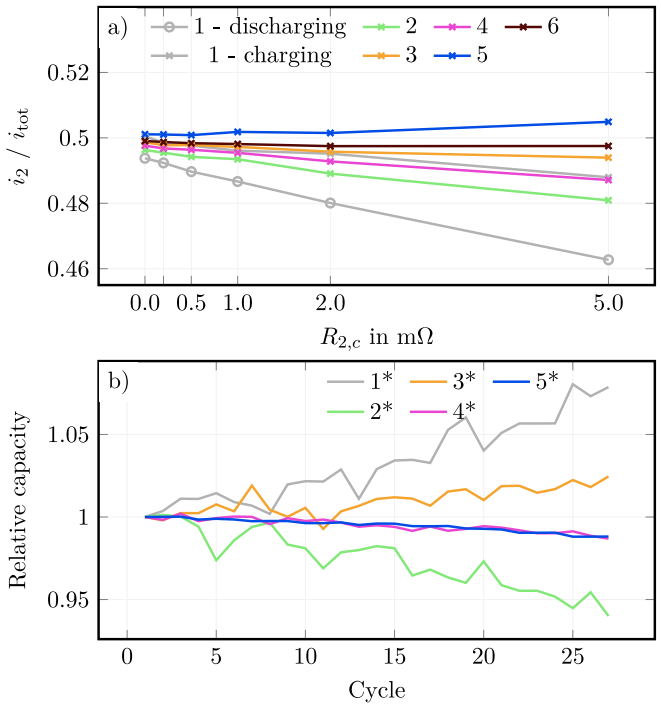

Fig. 7. Analysis of minima and maxima as well as intersection points of both currents. (a) shows the current spread at different points within different additional resistances due to an inhomogeneous load of Fig. 5. (b) shows the relative progress of intersection points of both currents according to Fig. 6 over all cycles within the investigation of homogeneous resistance in aspect to the loaded charge. (For interpretation of the references to colour in this figure legend, the reader is referred to the web version of this article.)

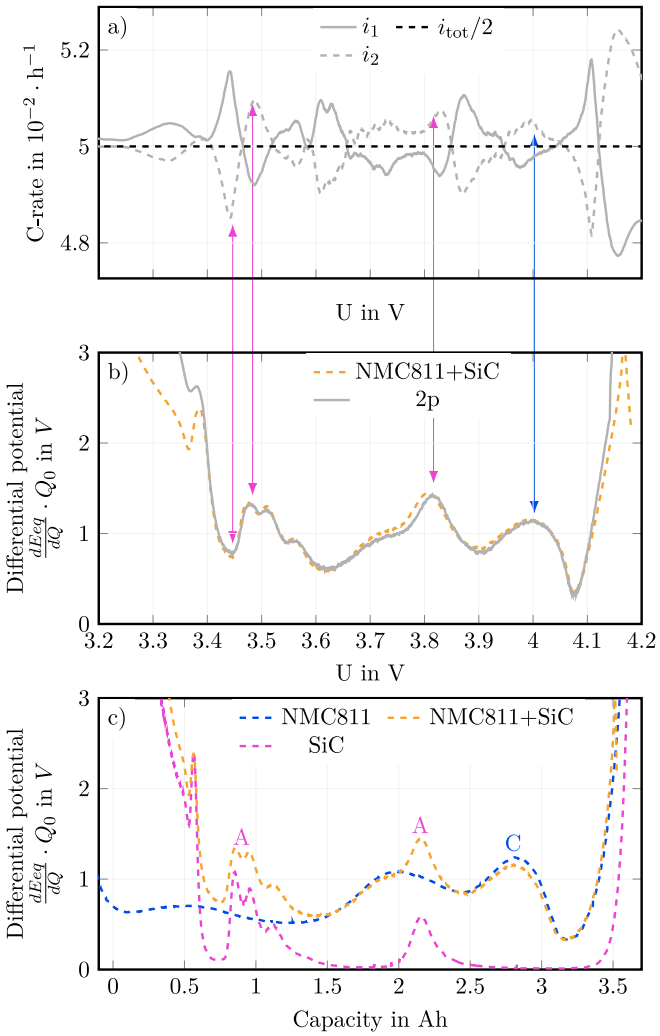

Fig. 8. Analysis of the DVA with the current distribution. (a) shows the current distribution between two parallel-connected cells with a homogeneous current in each branch of 0.05 C. The corresponding DVA during the 2p measurement is shown in (b). Additionally, the dashed lines in (b) and (c) were extracted from [53] and correspond to the half cell profiles and full cells of this cell type with assigned characteristic material markers. The arrows show some areas where the local minima and maxima between the current i_2 and DVA appear on the same voltage level. (For interpretation of the references to colour in this figure legend, the reader is referred to the web version of this article.)

et al. [53] and illustrate the contribution of the SiC anode and the nickel-rich NMC cathode to the DVA of the full cell. The dashed yellow lines in Fig. 8(b) and (c) correspond to the same measurement data, whereby the x-axis is set to voltage in Fig. 8(b) and to capacity in (c). For a better comparison, the data of the 2p measurement is shifted on the x-axis to match with data of [53]. Although the cell batch and the measurement current in this work and in [53] differ, the corresponding DVA during the 2p measurement and the full cell of [53] show similarities, see Fig. 8(b).

Even though the current distribution of the 2p measurement shows more characteristics peaks compared to the DVA, some local minima and maxima within the current through path 2, i_2, appear in almost the same region as the local minima and maxima of the 2p DVA. By assigning different peaks of both half cell profiles of the DVA to the anode and the cathode, see Fig. 8(c), the current distribution of both currents should be affected by these characteristic peaks. The pink arrows correspond to significant peaks belonging to the cathode and the blue arrows correspond to significant points belonging to the cathode. A clear explanation of the shape at low currents in Fig. 8 is still pending and will be continued in a subsequent work.

Additional ongoing investigations will focus on the development of the intersection points of both currents as a function of ageing. Nevertheless, the results of this work allow the conclusion, that the resistance ratio is responsible for the values of the local minima and maxima, whilst the DVA defines the shape of the current distribution.

4. Conclusion

This work presented a novel measurement technique to investigate the current distribution in parallel-connected cells. The cells were connected in parallel using Kirchhoff's laws and a battery cycler. By using the 4-wire measurement technique for each cell, the influence of system parameters such as interconnections and measurement equipment could be neglected, as is important for an exact and reproducible measurement setup. The novel measurement method was validated using a conventional test bench in charge and in discharge phases within CC, CV and resting periods. Measurement data showed good qualitative and quantitative agreement between the two measurement setups in regard to the local minima and maxima as well as the intersection points of both currents. The RMS was calculated to compare the measurements and showed low deviations of approximately 0.11 % across various charging phases and approximately 0.45 % across corresponding discharge phases.

To understand the influence of additional resistances in two parallel-connected cells, two measurement studies were carried out in which interconnection resistances were varied from 0 mΩ to 5 mΩ. Study one investigated the influence of an additional resistance in one parallel path, whilst study two addresses the influence of additional resistances in both parallel paths. The conclusion of both studies is, that the height of the local minima and maxima are mainly dependent on the

resistance ratio. They divide relative to the ratio of the combined cell and interconnection resistance in each pathway. In contrast, neither the local minima and maxima measured at various cumulative charge throughputs nor the intersection points of the current distribution are affected by varied resistances. OCV interactions between both cells determine the shape of the current distribution. Additionally, the shape of the DVA showed correlations with current distribution.

Using the tools set out in this work, the driving forces for convergence and divergence of the current distribution can be determined. As the cells are only ever connected in parallel via equations, it is possible to decouple the cells for check-ups and recouple them for cycling without ever touching them. This avoids any alteration of the contact resistance [4]. Additionally, with the flexibility of the virtual parallel connection, different cell formats can be investigated with less effort.

Based on the findings of these work, additional studies should be carried out. Ongoing work will focus on the ageing behaviour of parallel connected LIBs, influence of other electrode chemistry combinations as well as further analysis of the correlation between DVA, the intersection points of both currents and current distribution.

CRediT authorship contribution statement

P. Jocher: Conceptualization, Methodology, Software, Project administration, Writing - original draft, Visualization, Data curation, Investigation, Writing - review & editing. **M. Steinhardt:** Conceptualization, Writing - review & editing. **S. Ludwig:** Conceptualization, Writing - review & editing. **M. Schindler:** Writing - review & editing. **J. Martin:** Software, Conceptualization, Writing - review & editing. **A. Jossen:** Writing - review & editing, Supervision.

Declaration of competing interest

The authors declare that they have no known competing financial interests or personal relationships that could have appeared to influence the work reported in this paper.

Acknowledgements

Received funding from the Bavarian Research Foundation of the project OparaBatt, Germany (AZ-1296-17) and supported by the German Federal Ministry of Education and Research (BMBF), Germany under grant number 03XP0330A-F (OSLiB) is gratefully acknowledged. The responsibility for this publication rests with the authors.

References

[1] L. Noel, G. Zarazua de Rubens, B.K. Sovacool, J. Kester, Fear and loathing of electric vehicles: The reactionary rhetoric of range anxiety, Energy Res. Soc. Sci. 48 (2019) 96–107, http://dx.doi.org/10.1016/j.erss.2018.10.001.

[2] B. Tarroja, L. Zhang, van Wifvat, B. Shaffer, S. Samuelsen, Assessing the stationary energy storage equivalency of vehicle-to-grid charging battery electric vehicles, Energy 106 (2016) 673–690, http://dx.doi.org/10.1016/j.energy.2016.03.094.

[3] S. Kasap, P. Capper, Springer Handbook of Electronic and Photonic Materials, Springer International Publishing, Cham, 2017, http://dx.doi.org/10.1007/978-3-319-48933-9.

[4] M.J. Brand, P. Berg, E.I. Kolp, T. Bach, P. Schmidt, A. Jossen, Detachable electrical connection of battery cells by press contacts, J. Energy Storage 8 (2016) 69–77, http://dx.doi.org/10.1016/j.est.2016.09.011.

[5] A. Fill, T. Mader, T. Schmidt, R. Llorente, K.P. Birke, Measuring test bench with adjustable thermal connection of cells to their neighbors and a new model approach for parallel-connected cells, Batteries 6 (1) (2020) 2, http://dx.doi.org/10.3390/batteries6010002.

[6] M.H. Hofmann, K. Czyrka, M.J. Brand, M. Steinhardt, A. Noel, F.B. Spingler, A. Jossen, Dynamics of current distribution within battery cells connected in parallel, J. Energy Storage 20 (2018) 120–133, http://dx.doi.org/10.1016/j.est.2018.08.013.

[7] M.P. Klein, J.W. Park, Current distribution measurements in parallel-connected lithium-ion cylindrical cells under non-uniform temperature conditions, J. Electrochem. Soc. 164 (9) (2017) A1893–A1906, http://dx.doi.org/10.1149/2.0011709jes.

[8] Z. Wei, J. Zhao, H. He, G. Ding, H. Cui, L. Liu, Future smart battery and management: Advanced sensing from external to embedded multi-dimensional measurement, J. Power Sources 489 (1) (2021) 229462, http://dx.doi.org/10.1016/j.jpowsour.2021.229462.

[9] F. An, J. Huang, C. Wang, Z. Li, J. Zhang, S. Wang, P. Li, Cell sorting for parallel lithium-ion battery systems: Evaluation based on an electric circuit model, J. Energy Storage 6 (2016) 195–203, http://dx.doi.org/10.1016/j.est.2016.04.007.

[10] T. Bruen, J. Marco, Modelling and experimental evaluation of parallel connected lithium ion cells for an electric vehicle battery system, J. Power Sources 310 (2016) 91–101, http://dx.doi.org/10.1016/j.jpowsour.2016.01.001.

[11] M. Dubarry, A. Devie, B.Y. Liaw, Cell-balancing currents in parallel strings of a battery system, J. Power Sources 321 (2016) 36–46, http://dx.doi.org/10.1016/j.jpowsour.2016.04.125.

[12] A. Fill, T. Schmidt, T. Mader, R. Llorente, A. Avdyli, B. Mulder, K.P. Birke, Influence of cell parameter differences and dynamic current stresses on the current distribution within parallel-connected lithium-ion cells, J. Energy Storage 32 (2020) 101929, http://dx.doi.org/10.1016/j.est.2020.101929.

[13] M. Fleckenstein, O. Bohlen, M.A. Roscher, B. Bäker, Current density and state of charge inhomogeneities in li-ion battery cells with lifepo4 as cathode material due to temperature gradients, J. Power Sources 196 (10) (2011) 4769–4778, http://dx.doi.org/10.1016/j.jpowsour.2011.01.043.

[14] R. Gogoana, M.B. Pinson, M.Z. Bazant, S.E. Sarma, Internal resistance matching for parallel-connected lithium-ion cells and impacts on battery pack cycle life, J. Power Sources 252 (2014) 8–13, http://dx.doi.org/10.1016/j.jpowsour.2013.11.101.

[15] X. Gong, R. Xiong, C.C. Mi, Study of the characteristics of battery packs in electric vehicles with parallel-connected lithium-ion battery cells, IEEE Trans. Ind. Appl. 51 (2) (2015) 1872–1879, http://dx.doi.org/10.1109/TIA.2014.2345951.

[16] T. Grün, K. Stella, O. Wollersheim, Influence of circuit design on load distribution and performance of parallel-connected lithium ion cells for photovoltaic home storage systems, J. Energy Storage 17 (2018) 367–382, http://dx.doi.org/10.1016/j.est.2018.03.010.

[17] I. Hunt, T. Zhang, Y. Patel, M. Marinescu, R. Purkayastha, P. Kovacik, S. Walus, A. Swiatek, G.J. Offer, The effect of current inhomogeneity on the performance and degradation of li-s batteries, J. Electrochem. Soc. 165 (1) (2018) A6073–A6080, http://dx.doi.org/10.1149/2.0141801jes.

[18] F. Hust, Physico-Chemically Motivated Parameterization and Modelling of Real-Time Capable Lithium-Ion Battery Models - a Case Study on the Tesla Model S Battery (Ph.D. thesis), RWTH AACHEN UNIVERSTIY, Aachen, 2018, http://dx.doi.org/10.18154/RWTH-2019-00249.

[19] S. Miyatake, Y. Susuki, T. Hikihara, S. Itoh, K. Tanaka, Discharge characteristics of multicell lithium-ion battery with nonuniform cells, J. Power Sources 241 (2013) 736–743, http://dx.doi.org/10.1016/j.jpowsour.2013.05.179.

[20] A.S. Mussa, M. Klett, G. Lindbergh, R.W. Lindström, Effects of external pressure on the performance and ageing of single-layer lithium-ion pouch cells, J. Power Sources 385 (2018) 18–26, http://dx.doi.org/10.1016/j.jpowsour.2018.03.020.

[21] C. Pastor-Fernández, T. Bruen, W.D. Widanage, M.A. Gama-Valdez, J. Marco, A study of cell-to-cell interactions and degradation in parallel strings: Implications for the battery management system, J. Power Sources 329 (2016) 574–585, http://dx.doi.org/10.1016/j.jpowsour.2016.07.121.

[22] Y. Pan, X. Feng, M. Zhang, X. Han, L. Lu, M. Ouyang, Internal short circuit detection for lithium-ion battery pack with parallel-series hybrid connections, J. Cleaner Prod. 255 (2020) 120277, http://dx.doi.org/10.1016/j.jclepro.2020.120277.

[23] W. Shi, X. Hu, C. Jin, J. Jiang, Y. Zhang, T. Yip, Effects of imbalanced currents on large-format lifepo 4 /graphite batteries systems connected in parallel, J. Power Sources 313 (2016) 198–204, http://dx.doi.org/10.1016/j.jpowsour.2016.02.087.

[24] G. Zhang, C.E. Shaffer, C.-Y. Wang, C.D. Rahn, In-situ measurement of current distribution in a li-ion cell, J. Electrochem. Soc. 160 (4) (2013) A610–A615, http://dx.doi.org/10.1149/2.046304jes.

[25] M. Zhang, M. Ouyang, L. Lu, X. He, X. Feng, L. Liu, X. Xie, Battery internal short circuit detection, ECS Trans. 77 (11) (2017) 217–223, http://dx.doi.org/10.1149/07711.0217ecst.

[26] Y. Zhang, J. Zheng, S. Lin, F. Bai, W.H. Tanveer, S. Cha, X. Wu, W. Feng, Nonuniform current distribution within parallel-connected batteries, Int. J. Energy Res. 42 (8) (2018) 2835–2844, http://dx.doi.org/10.1002/er.4039.

[27] M.J. Brand, P.A. Schmidt, M.F. Zaeh, A. Jossen, Welding techniques for battery cells and resulting electrical contact resistances, J. Energy Storage 1 (2015) 7–14, http://dx.doi.org/10.1016/j.est.2015.04.001.

[28] M.J. Brand, M.H. Hofmann, M. Steinhardt, S.F. Schuster, A. Jossen, Current distribution within parallel-connected battery cells, J. Power Sources 334 (2016) 202–212, http://dx.doi.org/10.1016/j.jpowsour.2016.10.010.

[29] M.J. Brand, E.I. Kolp, P. Berg, T. Bach, P. Schmidt, A. Jossen, Electrical resistances of soldered battery cell connections, J. Energy Storage 12 (2017) 45–54, http://dx.doi.org/10.1016/j.est.2017.03.019.

[30] P. Taheri, S. Hsieh, M. Bahrami, Investigating electrical contact resistance losses in lithium-ion battery assemblies for hybrid and electric vehicles, J. Power Sources 196 (15) (2011) 6525–6533, http://dx.doi.org/10.1016/j.jpowsour.2011.03.056.

[31] M. Baumann, L. Wildfeuer, S. Rohr, M. Lienkamp, Parameter variations within li-ion battery packs – theoretical investigations and experimental quantification, J. Energy Storage 18 (2018) 295–307, http://dx.doi.org/10.1016/j.est.2018.04.031.

[32] S. Paarmann, L. Cloos, J. Technau, T. Wetzel, Measurement of the temperature influence on the current distribution in lithium–ion batteries, Energy Technol. 158 (2021) 2000862, http://dx.doi.org/10.1002/ente.202000862.

[33] J. Sturm, A. Rheinfeld, I. Zilberman, F.B. Spingler, S. Kosch, F. Frie, A. Jossen, Modeling and simulation of inhomogeneities in a 18650 nickel-rich, silicon-graphite lithium-ion cell during fast charging, J. Power Sources 412 (2019) 204–223, http://dx.doi.org/10.1016/j.jpowsour.2018.11.043.

[34] T.M.M. Heenan, A. Jnawali, M.D.R. Kok, T.G. Tranter, C. Tan, A. Dimitrijevic, R. Jervis, D.J.L. Brett, P.R. Shearing, An advanced microstructural and electrochemical datasheet on 18650 li-ion batteries with nickel-rich NMC811 cathodes and graphite-silicon anodes, J. Electrochem. Soc. 167 (14) (2020) 140530, http://dx.doi.org/10.1149/1945-7111/abc4c1.

[35] K. Rumpf, M. Naumann, A. Jossen, Experimental investigation of parametric cell-to-cell variation and correlation based on 1100 commercial lithium-ion cells, J. Energy Storage 14 (2017) 224–243, http://dx.doi.org/10.1016/J.EST.2017.09.010.

[36] I. Zilberman, S. Ludwig, A. Jossen, Cell-to-cell variation of calendar aging and reversible self-discharge in 18650 nickel-rich, silicon–graphite lithium-ion cells, J. Energy Storage 26 (2019) 100900, http://dx.doi.org/10.1016/j.est.2019.100900.

[37] M. Schindler, J. Sturm, S. Ludwig, J. Schmitt, A. Jossen, Evolution of initial cell-to-cell variations during a three-year production cycle, eTransportation (2021) 100102, http://dx.doi.org/10.1016/j.etran.2020.100102.

[38] M.H. Hofmann, Current Distribution in Parallel-Connected Battery Cells, Vol. 1, auflage ed., Verlag Dr. Hut, München, 2020, URL: https://www.dr.hut-verlag.de/9783843946148.html.

[39] A. Cordoba-Arenas, S. Onori, G. Rizzoni, A control-oriented lithium-ion battery pack model for plug-in hybrid electric vehicle cycle-life studies and system design with consideration of health management, J. Power Sources 279 (8) (2015) 791–808, http://dx.doi.org/10.1016/j.jpowsour.2014.12.048.

[40] P.-L. Huynh, Beitrag Zur Bewertung Des Gesundheitszustands Von Traktionsbatterien in Elektrofahrzeugen, Springer Fachmedien Wiesbaden, Wiesbaden, 2016, http://dx.doi.org/10.1007/978-3-658-16562-8.

[41] N. Kakimoto, K. Goto, Capacity-fading model of lithium-ion battery applicable to multicell storage systems, IEEE Trans. Sustain. Energy 7 (1) (2016) 108–117, http://dx.doi.org/10.1109/TSTE.2015.2476476.

[42] S.F. Schuster, M.J. Brand, P. Berg, M. Gleissenberger, A. Jossen, Lithium-ion cell-to-cell variation during battery electric vehicle operation, J. Power Sources 297 (2015) 242–251, http://dx.doi.org/10.1016/j.jpowsour.2015.08.001.

[43] C.R. Birkl, M.R. Roberts, E. McTurk, P.G. Bruce, D.A. Howey, Degradation diagnostics for lithium ion cells, J. Power Sources 341 (1) (2017) 373–386, http://dx.doi.org/10.1016/j.jpowsour.2016.12.011.

[44] R.A. Maronna, D.R. Martin, V.J. Yohai, M. Salibián-Barrera, Robust Statistics: Theory and Methods (with R), second ed., in: Wiley Series in Probability and Statistics Ser, John Wiley & Sons Incorporated, Newark, 2018, URL: https://ebookcentral.proquest.com/lib/gbv/detail.action?docID=5568377.

[45] S. Gantenbein, M. Weiss, E. Ivers-Tiffée, Impedance based time-domain modeling of lithium-ion batteries: Part i, J. Power Sources 379 (2018) 317–327, http://dx.doi.org/10.1016/j.jpowsour.2018.01.043.

[46] W. Waag, S. Käbitz, D.U. Sauer, Experimental investigation of the lithium-ion battery impedance characteristic at various conditions and aging states and its influence on the application, Appl. Energy 102 (2013) 885–897, http://dx.doi.org/10.1016/j.apenergy.2012.09.030.

[47] I. Zilberman, J. Schmitt, S. Ludwig, M. Naumann, A. Jossen, Simulation of voltage imbalance in large lithium-ion battery packs influenced by cell-to-cell variations and balancing systems, J. Energy Storage 32 (2020) 101828, http://dx.doi.org/10.1016/j.est.2020.101828.

[48] H.-J. Noh, S. Youn, C.S. Yoon, Y.-K. Sun, Comparison of the structural and electrochemical properties of layered li[nixcoymnz]o2 (x = 1/3, 0.5, 0.6, 0.7, 0.8 and 0.85) cathode material for lithium-ion batteries, J. Power Sources 233 (2013) 121–130, http://dx.doi.org/10.1016/j.jpowsour.2013.01.063.

[49] D. Anseán, G. Baure, M. González, I. Cameán, A.B. García, M. Dubarry, Mechanistic investigation of silicon-graphite/lini0.8mn0.1co0.1o2 commercial cells for non-intrusive diagnosis and prognosis, J. Power Sources 459 (2020) 227882, http://dx.doi.org/10.1016/j.jpowsour.2020.227882.

[50] P. Keil, S.F. Schuster, J. Wilhelm, J. Travi, A. Hauser, R.C. Karl, A. Jossen, Calendar aging of lithium-ion batteries, J. Electrochem. Soc. 163 (9) (2016) A1872–A1880, http://dx.doi.org/10.1149/2.0411609jes.

[51] M. Dubarry, C. Truchot, B.Y. Liaw, Synthesize battery degradation modes via a diagnostic and prognostic model, J. Power Sources 219 (2012) 204–216, http://dx.doi.org/10.1016/j.jpowsour.2012.07.016.

[52] I. Bloom, A.N. Jansen, D.P. Abraham, J. Knuth, S.A. Jones, V.S. Battaglia, G.L. Henriksen, Differential voltage analyses of high-power, lithium-ion cells, J. Power Sources 139 (1–2) (2005) 295–303, http://dx.doi.org/10.1016/j.jpowsour.2004.07.021.

[53] J. Sturm, A. Frank, A. Rheinfeld, S.V. Erhard, A. Jossen, Impact of electrode and cell design on fast charging capabilities of cylindrical lithium-ion batteries, J. Electrochem. Soc. 167 (13) (2020) 130505, http://dx.doi.org/10.1149/1945-7111/abb40c.